PNAS Nexus, 2023, 2, 1–8
https://doi.org/10.1093/pnasnexus/pgad391
Advance access publication 14 November 2023
Research Report

Observing network effect of shipping emissions from space: A natural experiment in the world's busiest port

Song Liu[a], Xicheng Li[a], Juan Li[a], Lei Shu[b], Tzung-May Fu[a,c,d], Xin Yang[a,c,d] and Lei Zhu[a,c,d,*]

[a]School of Environmental Science and Engineering, Southern University of Science and Technology, Shenzhen 518055, China
[b]School of Geographical Sciences, Fujian Normal University, Fuzhou 350007, China
[c]Guangdong Provincial Observation and Research Station for Coastal Atmosphere and Climate of the Greater Bay Area, Shenzhen 518055, China
[d]Shenzhen Key Laboratory of Precision Measurement and Early Warning Technology for Urban Environmental Health Risks, School of Environmental Science and Engineering, Southern University of Science and Technology, Shenzhen 518055, China
*To whom correspondence should be addressed: Email: zhul3@sustech.edu.cn
Edited By: Chris Muris

Abstract

Maritime trade and associated emissions are dynamic in nature. Although shipping emissions contribute significantly to air quality and climate change, their trade-governed dynamics remain less explored due to the lack of observational evidence. Here, we use satellite measurements to capture the redistribution of shipping nitrogen oxides (NO_x) emissions from Shanghai port, the world's busiest port, during a natural experiment posted by the localized COVID-19 lockdown in 2022. Viewing the ports as nodes in a network linked by ship journeys, we quantify a lockdown-induced −42% reduction in shipping NO_x emissions for Shanghai port. We further identify an emission transfer to its neighboring connected ports, confirmed by comprehensive vessel activity observations. Our study highlights the socioeconomic drivers of shipping emissions, which may add additional layers of complexity to air quality management.

Keywords: satellite remote sensing, shipping NO_x emission, network effect, emission transfer

Significance Statement

Maritime trade and associated emissions are dynamic in nature. Although shipping emissions contribute significantly to air quality and climate change, their trade-governed dynamics remain less explored due to the lack of observational evidence. Viewing the ports as nodes in a network linked by ship journeys, we use satellite measurements to capture redistribution of shipping NO_x emissions from Shanghai port to its neighboring connected ports, during a natural experiment posted by the localized COVID-19 lockdown. Our study highlights the socioeconomic drivers of shipping emissions, which may add additional layers of complexity to air quality management.

Introduction

In global supply chains, centers of production and consumption create a complex network of trade flows. With large carrying capacity, high safety, and low operating cost, maritime transport accounts for >80% of the world's trade by volume and is projected to increase at an annual rate of 2.1% up to 2027 (1). The associated air pollutant emissions, however, have become a nonneglectable issue against worldwide emission reduction and climate change goals (2, 3), at both global and regional levels. Large-scale shipping emission transfer embodied in international trade has been previously evaluated in bottom-up inventories (4, 5). In contrast, detailed dynamic features of trade-linked shipping emissions are less studied. Here, we provide the first observational evidence from space to the near-real-time variations in air pollutants, which are governed by the network structure of maritime connections, i.e. ship trajectories can be interpreted as a directed network where the nodes are ports linked by shipping activities (6).

Nitrogen oxides ($NO_x \equiv NO + NO_2$) emissions from global shipping fleet account for 15 to 35% of total anthropogenic NO_x emissions (7, 8). NO_x deteriorates coastal air quality and influences climate change as a primary pollutant with adverse health outcomes (9, 10) and as a precursor to ozone and fine particular matter (11). Due to the important influences of shipping NO_x emissions, bottom-up inventories based on big data from a ship's automatic identification system (AIS) have received increasing attention (8, 12–15). However, such inventories are typically time-consuming and potentially subject to large uncertainties due to the difficulty in determining shipping activities and emission factors (16, 17).

Satellite-based NO_2 observations have been widely used to detect busy ship tracks and constrain shipping NO_x emissions (18–20). Since 2007, Global Ozone Monitoring Experiment-2 (GOME-2) aboard the Metop series of satellites (21, 22) has been continuously providing global measurements of tropospheric

Competing Interest: The authors declare no competing interest.
Received: May 8, 2023. **Accepted:** November 7, 2023

NO_2 columns with a high signal-to-noise ratio (23). The new-generation spectrometer TROPOspheric Monitoring Instrument (TROPOMI) onboard the Copernicus Sentinel 5 Precursor satellite (24), meanwhile, observes global NO_2 at an unprecedented spatial resolution (up to 5.6km × 3.6km), offering a unique capability to pinpointing fine-scale NO_x emissions over ship tracks (25, 26).

Despite the crucial importance of maritime logistics to the global economy and the rapid development of satellite spectrometers, top-down evidence of the linkage between shipping emissions and maritime trade, as well as their socioeconomic drivers, remains unexplored. The 2022 COVID-19 Shanghai lockdown provides a rare natural experiment, in which the world's largest and busiest port is affected by restrictive measures starting initially in mid-March. From April 1 to May 31, human mobility, public transportation, and manufacturing are significantly reduced under city-wide stay-at-home protection and staggered-shift policies. In spite of the continuous operation, Shanghai port is interfered by disruptions of supply chain and road transportation. Viewing the global ports as nodes in a trade network linked by ship journeys, the partial closure of Shanghai port forces an adaption of maritime traffic flows to its connected ports, following network-based affinities such as distance and economic ties (6, 27).

In this work, we begin by employing GOME-2/MetOp-B (throughout this study referred to as GOME-2B) and TROPOMI satellite measurements to monitor NO_2 variations during the lockdown. We next apply a mass-balance approach to infer shipping NO_x emissions based on Goddard Earth Observing System (GEOS)-Chem chemical transport model simulations. Finally, the derived temporal variations are verified with observed ship journeys to understand the maritime network evolution and the role of such traffic redistribution on air quality. Our work provides new implications for emission control, where environmental policies require explicitly accounting for the dynamic geographical transfer of trade-related air pollution emissions.

Results and discussion

Shipping NO_x emission variations in response to the lockdown

Satellites clearly capture high values of tropospheric NO_2 columns by $>2.0 \times 10^{15}$ molecules cm^{-2} over ship tracks over the Chinese seas in April–May 2022, reflecting the general good data quality of GOME-2B (Fig. 1a) and TROPOMI (Supplementary Fig. S1a). Comparing the two satellite datasets, tropospheric NO_2 columns from GOME-2B are higher than TROPOMI observations by about 1.0×10^{15} molecules cm^{-2}, mainly mirroring the longer chemical lifetime of NO_x in the midmorning (9:30 local time for GOME-2B) than the early afternoon (13:30 local time for TROPOMI) [Supplementary Fig. S2; (28)]. Additionally, the differences are contributed by retrieval differences, such as the stratospheric correction and cloud treatment (29–33).

GOME-2B tropospheric NO_2 columns over the surrounding water of Shanghai start to decline in mid-March 2022 (Fig. 1c), when the government imposes initial lockdown restrictions (Fig. 1d). Compared with the previous year under business-as-usual conditions, the tropospheric NO_2 columns over Shanghai port decrease by $-3.2 \pm 1.1 \times 10^{15}$ molecules cm^{-2} ($-30.6 \pm 9.8\%$) on average during April–May and rebound to the same levels in June (the abrupt reduction in early March 2021 is due to the late Spring Festival holiday). This reduction far exceeds the interannual variation ($\pm 1.0 \times 10^{15}$ molecules cm^{-2} or $\pm 9.4\%$ yr^{-1} estimated using GOME-2B climatology in 2013–2019), reflecting the reduced anthropogenic shipping activities in response to the lockdown and meteorological variations. In contrast, we notice NO_2 enhancements by up to 0.9×10^{15} molecules cm^{-2} (29.1%) over the shipping lanes between Shanghai and connected ports in North and East China (Fig. 1b), where the Oxford Stringency Index differences between the 2 years are typically <30 (except for Tangshan with a city-wide lockdown in March–May 2022).

Such positive variations in GOME-2 results (Fig. 1b) are less obvious in TROPOMI data (Supplementary Fig. S1b), mainly resulted from the lower instrumental signal-to-noise ratio, data sampling differences, the photochemical loss of NO_2 in the afternoon, as well as variable metrological conditions. Meteorological changes between April–May 2022 and 2021 contribute to NO_2 reductions by up to $-1.1 \pm 0.3 \times 10^{15}$ molecules cm^{-2} ($-13.9 \pm 3.9\%$) for GOME-2 and $-1.4 \pm 0.4 \times 10^{15}$ molecules cm^{-2} ($-19.8 \pm 4.2\%$) for TROPOMI over East China, calculated with GEOS-Chem using consistent anthropogenic emissions that exclude lockdown-attributable changes (Supplementary Fig. S3). Meanwhile, meteorology alone favors more strongly the NO_2 accumulations over shipping lanes connecting Shanghai and North China for GOME-2 (by up to $1.2 \pm 0.4 \times 10^{15}$ molecules cm^{-2} or $16.1 \pm 5.4\%$) than TROPOMI (by up to $0.4 \pm 0.1 \times 10^{15}$ molecules cm^{-2} or $2.1 \pm 0.5\%$).

Roles of network effect in redistributing shipping NO_x emissions

Maritime trade flows and associated shipping NO_x emissions are governed by the network effect. In response to the localized lockdown, the vessels originally supposed to flow to Shanghai have to be redirected to connected ports, depending on network features such as distance and port throughput. Estimated with the port gravity model (27) considering sea distances and the observed total numbers of ship arrivals and departures at major Chinese ports, the Shanghai port shares trade connections mostly with ports in North China as well as the Ningbo-Zhoushan port cluster (Supplementary Fig. S4), which are potential places taking over vessels from Shanghai.

Evolution of the maritime network is followed by emission transfer, for which the near-real-time top-down information from satellites represents an attractive means of supplementing bottom-up emission inventories. Satellite-constrained shipping NO_x emissions for Shanghai port are $2.2 \pm 1.9 \times 10^{-10}$ kg m^{-2} s^{-1} (GOME-2B) and $1.1 \pm 1.4 \times 10^{-10}$ kg m^{-2} s^{-1} (TROPOMI) in April–May 2021, generally agree with state-of-the-art inventories with $1.0 \pm 0.3 \times 10^{-11}$, $0.9 \pm 1.5 \times 10^{-10}$, and $1.5 \pm 1.8 \times 10^{-10}$ kg m^{-2} s^{-1} from CEDS v2021 (34), EDGAR v6.1 (8, 35), and CAMS-GLOB-SHIP v2.1 (13), respectively (Supplementary Fig. S5). Bottom-up uncertainties arise from assumptions about emission drivers (such as fuel consumption) or availability and quality of AIS data (12).

During the lockdown period, the GOME-2B shipping NO_x emissions decrease by $-9.2 \pm 8.4 \times 10^{-11}$ kg m^{-2} s^{-1} ($-41.7 \pm 15.3\%$) over Shanghai port (Fig. 2a), as a consequence of reduced maritime transport activities both for domestic and foreign trade (Fig. 2b). This is consistent with observations of ship journeys and statistics of cargo throughput. Specifically, the AIS-based domestic shipping activities from Shanghai port reduce by −15,958 ship/times (−46%), and the reported domestic cargo throughput reduces by −18 million tonnes (−37%; Supplementary Fig. S6; Ministry of Transport of the People's Republic of China; https://mot.gov.cn). Reductions in Shanghai's shipping activities are mainly related to ship arrivals rather than departures, as shown in the detailed records of single-direction connections between pairs of major Chinese ports (Supplementary Fig. S7).

Meanwhile, carriers supposed to arrive at Shanghai reroute to connected ports such as Qingdao and Ningbo-Zhoushan (1),

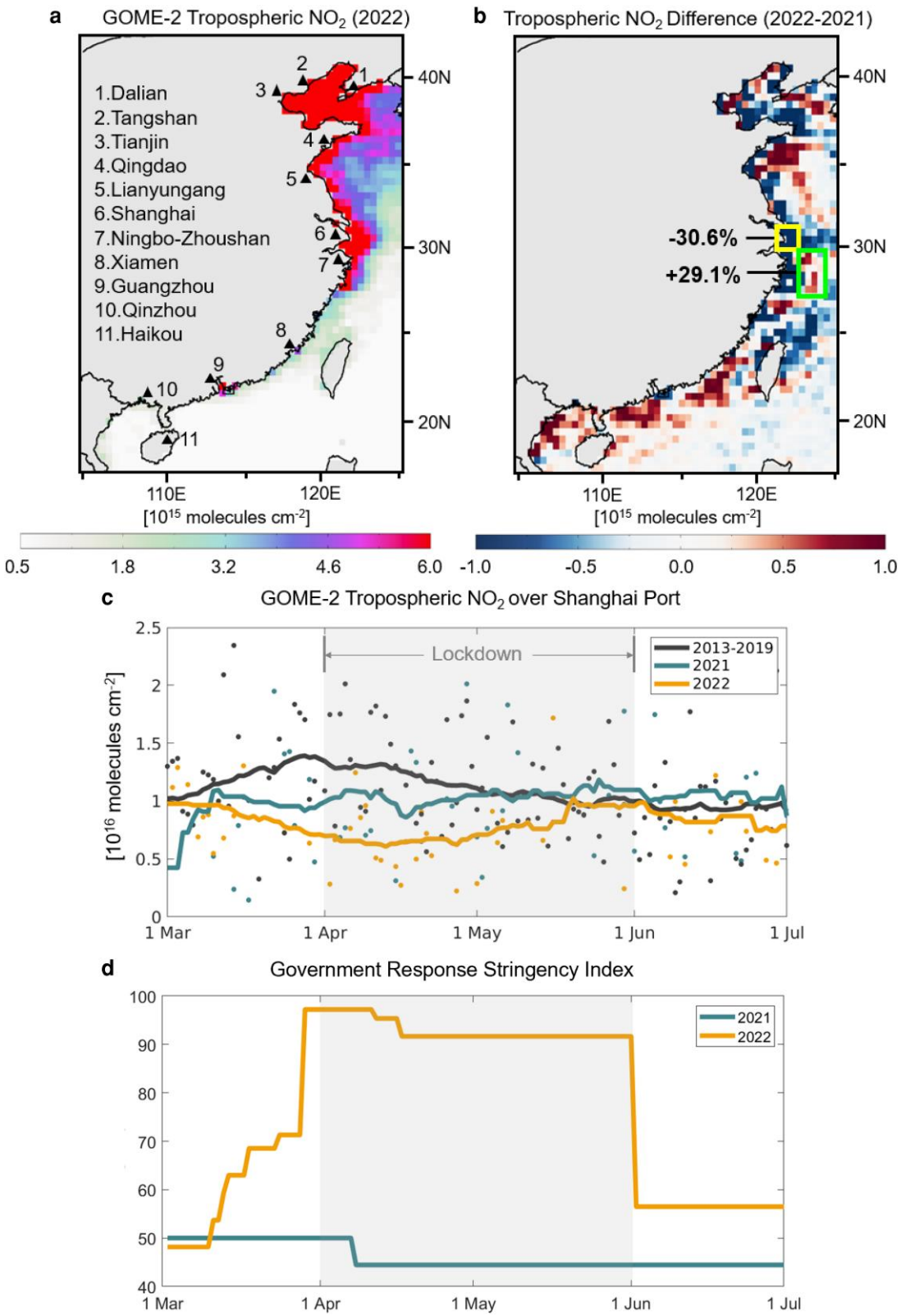

Fig. 1. Variations in tropospheric NO_2 columns near China seas in response to COVID-19 lockdown. a) GOME-2B tropospheric NO_2 columns during April–May 2022. b) GOME-2B tropospheric NO_2 differences compared with the same period in 2021. c) 28-Day moving averages of GOME-2B tropospheric NO_2 columns over Shanghai port in 2013–2019, 2021, and 2022. d) The Oxford COVID-19 Government Response Stringency Index (https://www.bsg.ox.ac.uk/research/covid-19-government-response-tracker#data) in 2021 and 2022. Triangles, indexes, and names in panel a mark the top port in each coastal province in China. Boxes indicate Shanghai (30.6°N–31.5°N, 121.2°E–122.5°E) and Ningbo-Zhoushan (28.5°N–30.6°N, 122.5°E–124.0°E) port regions with relative changes in tropospheric NO_2 columns given inset.

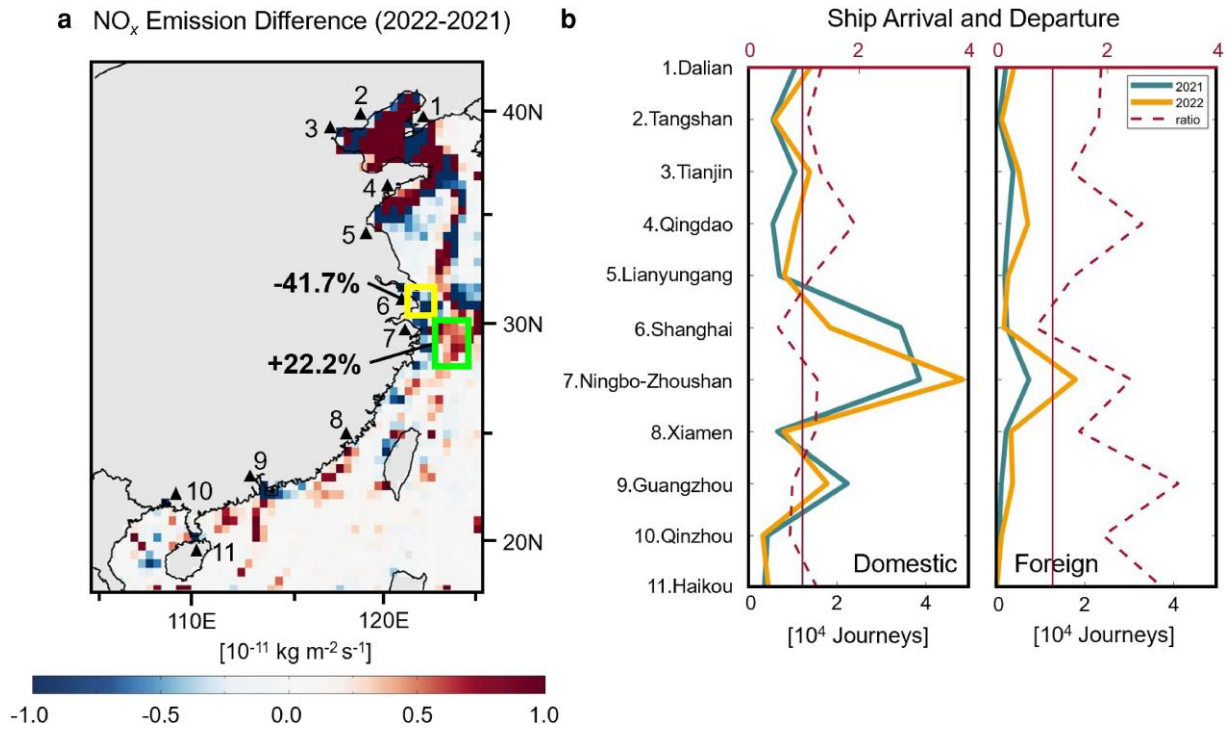

Fig. 2. Network evolutions of maritime trade and shipping NO_x emissions. a) Differences in shipping NO_x emissions constrained by GOME-2B satellite data during the 2022 lockdown relative to the same period in 2021. b) Observed total numbers of ship arrivals and departures for the top port in each coastal province in China. Boxes indicate Shanghai and Ningbo-Zhoushan port regions with relative changes in shipping NO_x emissions given inset. Dashed lines in panel b show the ratio of 2022 to 2021. Solid lines mark the line of equality.

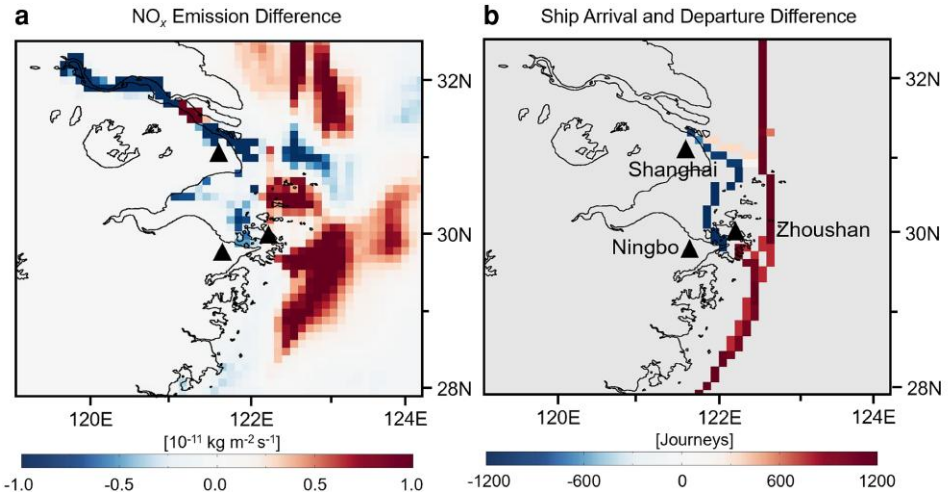

Fig. 3. Transfer of shipping NO_x emissions from Shanghai to Ningbo-Zhoushan. a) Differences in shipping NO_x emissions constrained by TROPOMI data during the 2022 lockdown relative to the same period in 2021. b) Differences in ship arrivals and departures between all pairs of top ports in each coastal province. Triangles mark the locations of Shanghai, Ningbo, and Zhoushan. Ship arrival and departure differences (Supplementary Fig. S7b) are summed up over each ship trajectory (obtained from https://www.hifleet.com) in panel b.

transportation and logistic centers in North and East China, respectively. In particular for Ningbo-Zhoushan, which generates a subnetwork of vessel flows with the adjacent Shanghai port, the traffic redistribution witnesses an increase in domestic ship arrivals and departures by 9,642 ship/times (corresponding to about 60% traffic loss by Shanghai; Fig. 2b) and consequently an increase in GOME-2B shipping NO_x emissions by $2.8 \pm 2.3 \times 10^{-11}$ kg m^{-2} s^{-1} ($22.2 \pm 17.8\%$; Fig. 2a). Despite that similar variations in ship journeys (Fig. 2b) and cargo throughput (Supplementary Fig. S6) are also observed for foreign trade, these ocean-going shipping activities, complicated by longer traveling time, geopolitical environment (e.g. the Russia–Ukraine conflict), or economic situations of other countries, are excluded for further quantifications.

The unprecedented spatial resolution of TROPOMI (up to $5.6\text{km} \times 3.6\text{km}$) enables the direct assessment of NO_x variations over individual ports. Along the major ship tracks, TROPOMI shipping NO_x emissions reduce by up to −29.3% for Shanghai and enhance by up to 44.9% for Ningbo-Zhoushan (Fig. 3a), consistent

with variations in ship arrivals and departures between major port pairs (Fig. 3b). Despite differences in signal-to-noise ratio, overpass time, and data sampling, the TROPOMI-based emission changes are generally in line with GOME-2B results (Fig. 2a) but at lower magnitudes with similar reasons as analyzed for Fig. 1. Nevertheless, satellite evidences show that the traffic redistribution after the lockdown is dynamically absorbed by the subnetwork of trade, resulting in an intermediate transfer in shipping NO_x emissions.

Impact of transferred shipping NO_x emissions on air quality

Our findings about shifted shipping NO_x emissions raise the interest in assessing their role in forming secondary pollution over port cities. With satellite-constrained emissions, we perform GEOS-Chem sensitivity simulations to quantify the impacts of transferred shipping NO_x emissions on surface daily maximum 8 h average (MDA8) ozone. Figure 4 shows the mean differences between the base simulation in April–May 2022 with business-as-usual emissions and a sensitivity simulation with locally perturbated emissions from Fig. 3a. Due to the nonlinear ozone chemistry, ozone level increases by up to 2.8 μg cm^{-3} (2.2%) over Shanghai and experiences a degradation by up to −3.2 μg cm^{-3} (−2.6%) over Ningbo-Zhoushan, likely determined by the locally reduced/enhanced NO_x-titration effect under the NO_x-saturated regime (36). It is noted that our conclusions can be regarded as lower limits of variations of shipping NO_x emissions and ozone concentrations, as the "business-as-usual" year 2021 is also affected by COVID-19 and lockdown measures to a certain degree (Fig. 1d). For instance, the climatological increases in tropospheric NO_2 columns before April, likely due to the increased fishing activities (19), are not observed in 2021 (Fig. 1c).

Although our analysis focuses on one localized event in China, our results are relevant beyond the case. Extreme cases, such as closures of the Iskenderun port after the 2023 Turkey earthquake or the Suez Canal after the 2021 obstruction accident, experience similar adaptions of traffic flows. Within the network structure of sea connections, voyages divert to the nearby Turkish Yumutalik/Mersin ports (37) or reroute around the Cape of Good Hope in South Africa (38), respectively, introducing distinct NO_2 pollution transfers (Supplementary Figs. S8 and S9).

In summary, our work underlines the complex behavior of the maritime trade network and its influences on local air quality, providing important implications for emission control. Despite the increasingly strict emission control and consequent improvements in fuel quality and engine technology, global shipping NO_x emissions have continued to increase (5). Management of vessel routes is expected to influence air quality over coastal or sensitive areas locally and regionally. In particular for these regions, environmental policies require explicitly accounting for the dynamic geographical transfer of trade-related air pollution emissions. As such near-real-time variations are typically overlooked in emission inventories, satellite observations have the potential to play a critical role in monitoring emission variations, elucidating drivers, and enforcing regulations, particularly with the launch of a geostationary air quality constellation including Geostationary Environment Monitoring Spectrometer (GEMS) over Asia, Tropospheric Emissions: Monitoring of Pollution (TEMPO) over North America, and Sentinel-4 over Europe.

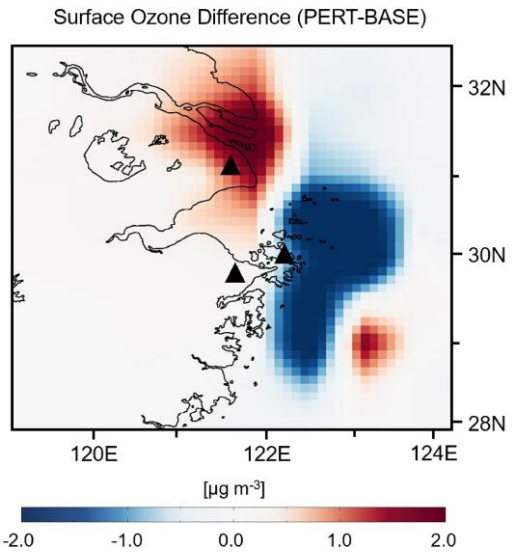

Fig. 4. Impacts of transferred shipping NO_x emission on surface ozone formation. Results are from the GEOS-Chem simulated changes in surface daily maximum 8 h average (MDA8) ozone from base simulation (BASE) to a perturbation simulation (PERT) in April–May 2022, conducted with shipping NO_x emissions constrained in Fig. 3a. Triangles mark the locations of Shanghai, Ningbo, and Zhoushan.

Materials and methods

GOME-2 and TROPOMI satellite measurements

GOME-2 and TROPOMI instruments are nadir-viewing spectrometers measuring the Earth's backscattered radiances and extraterrestrial solar irradiances. The GOME-2 instruments onboard the Meteorological Operational (MetOp-A, MetOp-B, and MetOp-C) satellites were launched in October 2006, September 2012, and November 2018, respectively. The default swath width of GOME-2B is 1,920 km, and the default ground pixel size is 80km × 40km in the forward scan. The TROPOMI sensor was launched in October 2017 aboard the ESA Sentinel-5 Precursor satellite. The swath width is 2,600 km in the direction across the track of the satellite, and the spatial resolution is 5.6km × 3.6km at nadir (7.2km × 3.6km before August 2019). The local equator crossing time is around 9:30 for GOME-2 and around 13:30 for TROPOMI. The signal-to-noise ratio in the NO_2 wavelength range is 4,000 for GOME-2B and 1,500 for TROPOMI.

We use the operational GOME-2 version GDP 4.8 data (ftp://acsaf.eoc.dlr.de) and TROPOMI version 02.03.01 data (offline for 2022; https://scihub.copernicus.eu; PAL reprocessing for 2021; https://data-portal.s5p-pal.com). Satellite NO_2 measurements are filtered for clouds (clouds radiance fraction <0.5) and aggregated based on an area-weighted tessellation to a resolution of 0.4° × 0.4° (GOME-2B) and 0.1° × 0.1° (TROPOMI). Satellite pixels significantly influenced by continental outflow are also removed, defined as data with >50% of 12-h air-mass back trajectories originating from the continents. We compute the back trajectories using the HYSPLIT model (39) at a spatial resolution of 2.5° × 2.5° and a temporal resolution of 6 h, driven by meteorological fields from the National Centers for Environmental Prediction (NCEP)/National Center for Atmospheric Research (NCAR) Reanalysis data (40, 41).

GOME-2 and TROPOMI single-pixel uncertainties, typically up to 60% for pollution scenes, are mainly introduced by spectral fitting, stratospheric correction, and air-mass factor calculation (29–33). GOME-2 and TROPOMI NO_2 products show similar negative biases of the order of −30 to −50% against ground-based observations, possibly influenced by different footprint sizes, retrieval uncertainties, and measurement sensitivities (42–44). Over coastal oceans, enhanced NO_2 levels (particularly in

morning hours) can be detected similarly by ship-based remote sensing instruments and satellite products (45).

GEOS-Chem model simulations

We run the chemical transport model GEOS-Chem version 12.9.3 (http://www.geos-chem.org) to simulate air pollutant concentrations at the satellite overpass time. The nested simulation over Asia (11°S–55°N, 60°E–150°E) is configured at a resolution of 0.5° × 0.625° with 47 vertical layers and boundary conditions updated every 3 h from a global 4° × 5° simulation. The global and nested simulations have a respective spin-up time of 1 year and 3 months, driven by Modern-Era Retrospective Analysis for Research and Applications, Version 2 (MERRA-2) meteorological fields (46).

Global anthropogenic emissions for the year 2018 are from the Hemispheric Transport of Air Pollution (HTAP) version 3 inventory (47, 48). The shipping sector of this global mosaic applies Emissions Database for Global Atmospheric Research (EDGAR) version 6.1 inventory, within which the shipping emissions apply new international shipping proxies and monthly profiles compared to the previous versions (8, 35). Our simulations accounts for the nonlinear in-plume chemistry of ship emissions by using the PARAmeterization of emitted NO_x (PARANOX) ship plume model (49, 50). Biogenic emissions are calculated online using Model of Emissions of Gases and Aerosols from Nature (MEGAN) version 2.1 (51). Biomass burning emissions are from the fourth-generation Global Fire Emissions Database (GFED4) (52).

The GEOS-Chem model is able to reproduce main patterns for trace gases with biases generally <50%, evaluated against extensive space-based, aircraft-based, and ground-based observations (53–55). As measurements over the ocean are scarce, we show in Supplementary Fig. S10 that our GEOS-Chem simulations agree with in situ NO_2 observations from the China National Environmental Monitoring Center (http://www.cnemc.cn/en), with correlation coefficients of 0.49 to 0.62 and mean biases of −4.5 to −22.8%. The biases are mainly related to the uncertainties in anthrophonic and natural emission estimates, along with the parameterization resolutions for meteorology or chemical processes (56). Reductions in 2022 in situ NO_2 concentrations can be partly attributed to the Shanghai lockdown, with city-wide averages decreasing from 34.0 μg m^{-3} in March–April 2021 to 21.4 μg m^{-3} in 2022 due to reduced anthropogenic NO_x emissions from road transportation and industrial processes (57).

For our emission estimates, nonshipping contributions from other anthropogenic sectors over the continent are relatively low, as we sample model results to valid satellite data that have been screening out for continental outflows. For the investigation of ozone pollution, however, the use of consistent nonshipping emissions in 2021 and 2022 potentially introduces uncertainties, as precursors are reported to reduce unevenly during the lockdown (57, 58). Nevertheless, our current conclusions remain relatively trustworthy, as Shanghai's urban region remains NO_x-saturated despite drastic reductions in NO_x emissions (58).

Shipping NO_x emission estimates

A finite difference mass-balance approach (59) is applied to estimate ship NO_x emissions from satellite NO_2 observations and model simulations. Based on GEOS-Chem simulations with EDGAR inventory as input for the shipping sector, we constrain top-down GOME-2B or TROPOMI shipping NO_x emissions E_{td} as:

$$E_{td} = E_{bu} + \frac{N_O - N_M}{N_M} \times \beta \times E_{bu}. \quad (1)$$

E_{bu} is the a priori shipping emissions from bottom-up EDGAR inventory. N_O and N_M indicate observed and modeled tropospheric NO_2 columns. The β-factor represents the local sensitivity of NO_2 column changes to NO_x emission changes, determined by perturbating the a priori ship inventory by the relative difference of observed and modeled NO_2 columns in Shanghai (30 ± 12%) (60).

Ship arrival and departure data

We obtain ship arrival and departure records for top ports in each Chinese coastal province during April–May in 2021 and 2022 from the commercial company HiFleet (https://www.hifleet.com). The data include total numbers of ship arrivals and departures (including domestic and foreign vessels) as well as detailed numbers of journeys between all pairs of the top ports. This vessel activity information is calculated based on AIS signals from shore-based stations (domestic China) or satellite-based systems (global). Minute-frequency AIS data include coordinate location, vessel type, voyage time, vessel draughts, and so on. We restrict our analysis to large ships, such as containers, bulk carriers, general cargo, and oil tankers, and we exclude fishing vessels because of the large uncertainty in AIS data and low shipping activities during the Moratorium of fishing.

Trade flow perdiction

Based on the total numbers of ship arrivals and departures, the trade flows F_{ij} can be predicted with the port gravity model (27) as:

$$F_{ij} = a_i b_j O_i I_j \times (d_{ij}^{-0.59} e^{-d_{ij}/4{,}900}). \quad (2)$$

O_i is the total number of departures from port i, and I_j is the number of arrivals at port j. The scaling coefficients a_i and b_j are obtained by ensuring $\sum_j F_{ij} = O_i$ and $\sum_i F_{ij} = I_j$. d_{ij} is the distance between ports i and j.

Supplementary Material

Supplementary material is available at *PNAS Nexus* online.

Funding

This work is funded by the National Natural Science Foundation for Young Scientists of China (42205134), Key-Area Research and Development Program of Guangdong Province (2020B1111360001), Shenzhen Key Laboratory of Precision Measurement and Early Warning Technology for Urban Environmental Health Risks (ZDSYS20220606100604008), Guangdong Basic and Applied Basic Research Foundation (2021A1515110713), Guangdong Basic and Applied Basic Research Fund (2020B1515130003), Guangdong University Research Project Science Team (2021KCXTD004), and Shenzhen Science and Technology Program (KQTD20210811090048025, JCYJ20210324104604012, JCYJ20220530115404009). This work is supported by the Center for Computational Science and Engineering at Southern University of Science and Technology.

Author Contributions

S.L. and L.Z. conceived the idea, conducted the analyses, and wrote the paper. X.L. and J.L. provided the data. L.S. interpreted the results. All authors contributed to the discussions and revisions of the manuscript.

Data Availability

The GOME-2 NO_2 data are available through the AC SAF FTP-server (ftp://acsaf.eoc.dlr.de). The operational TROPOMI/S5P NO_2 products are available via the Copernicus Open Access Hub (https://scihub.copernicus.eu). The reprocessed TROPOMI/S5P NO_2 products are available via the S5P-PAL Data Portal (https://data-portal.s5p-pal.com). The GEOS-Chem is available at http://www.geos-chem.org.

References

1 UNCTAD. 2022. Review of Maritime Transport 2022. United Nations Conference on Trade and Development (UNCTAD). Technical Report No. UNCTAD/RMT/2022. [accessed 2023 Oct 10]. https://unctad.org/publication/review-maritime-transport-2022.

2 Fuglestvedt J, Berntsen T, Myhre G, Rypdal K, Skeie RB. 2008. Climate forcing from the transport sectors. *Proc Natl Acad Sci U S A*. 105:454–458.

3 Liu H, *et al.* 2016. Health and climate impacts of ocean-going vessels in East Asia. *Nat Clim Change*. 6:1037–1041.

4 Du M,*et al.* 2022. Examining the sensitivity of global CO_2 emissions to trade restrictions over multiple years. *Environ Sci Technol Lett*. 9:293–298.

5 Wang X-T, *et al.* 2021. Trade-linked shipping CO_2 emissions. *Nat Clim Change*. 11:945–951.

6 Kosowska-Stamirowska Z. 2020. Network effects govern the evolution of maritime trade. *Proc Natl Acad Sci U S A*. 117:12719–12728.

7 Crippa M, *et al.* 2018. Gridded emissions of air pollutants for the period 1970–2012 within EDGAR v4.3.2. *Earth Syst Sci Data*. 10:1987–2013.

8 Johansson L, Jalkanen J-P, Kukkonen J. 2017. Global assessment of shipping emissions in 2015 on a high spatial and temporal resolution. *Atmos Environ*. 167:403–415.

9 Achakulwisut P, Brauer M, Hystad P, Anenberg SC. 2019. Global, national, and urban burdens of paediatric asthma incidence attributable to ambient NO_2 pollution: estimates from global datasets. *Lancet Planet Health*. 3:e166–e178.

10 Hamra GB, *et al.* 2015. Lung cancer and exposure to nitrogen dioxide and traffic: a systematic review and meta-analysis. *Environ Health Perspect*. 123:1107–1112.

11 Seinfeld JH, Pandis SN. 2016. *Atmospheric chemistry and physics: from air pollution to climate change*. Hoboken (NJ): John Wiley & Sons.

12 Jalkanen J-P, *et al.* 2009. A modelling system for the exhaust emissions of marine traffic and its application in the Baltic Sea area. *Atmos Chem Phys*. 9:9209–9223.

13 Jalkanen J-P, Johansson L, Kukkonen J. 2016. A comprehensive inventory of ship traffic exhaust emissions in the European sea areas in 2011. *Atmos Chem Phys*. 16:71–84.

14 Kukkonen J, *et al.* 2023. Towards a comprehensive evaluation of the environmental and health impacts of shipping emissions. In: Mensink C, Jorba O, editors. *Air pollution modeling and its application*, Vol. XXVIII. Cham: Springer. p. 329–336.

15 Weisheit J. 2023. THE SCIPPER PROJECT, shipping contributions to inland pollution push for the enforcement of regulations. European Commission. Technical Report No. D1.6 V1.0.

16 Wang C, Corbett JJ, Firestone J. 2007. Modeling energy use and emissions from North American shipping: application of the ship traffic, energy, and environment model. *Environ Sci Technol*. 41:3226–3232.

17 Zhang Y, *et al.* 2017. Shipping emissions and their impacts on air quality in China. *Sci Total Environ*. 581–582:186–198.

18 Beirle S, Platt U, Von Glasow R, Wenig M, Wagner T. 2004. Estimate of nitrogen oxide emissions from shipping by satellite remote sensing. *Geophys Res Lett*. 31:L18102.

19 Ding J, *et al.* 2018. Maritime NO_x emissions over Chinese seas derived from satellite observations. *Geophys Res Lett*. 45:2031–2037.

20 Richter A. 2004. Satellite measurements of NO_2 from international shipping emissions. *Geophys Res Lett*. 31:L23110.

21 Callies J, Corpaccioli E, Eisinger M, Hahne A, Lefebvre A. 2000. GOME-2-Metop's second-generation sensor for operational ozone monitoring. *ESA Bull*. 102:28–36.

22 Munro R, *et al.* 2016. The GOME-2 instrument on the Metop series of satellites: instrument design, calibration, and level 1 data processing—an overview. *Atmos Meas Tech*. 9:1279–1301.

23 Zara M, et al. 2018. Improved slant column density retrieval of nitrogen dioxide and formaldehyde for OMI and GOME-2A from QA4ECV: intercomparison, uncertainty characterisation, and trends. *Atmos Meas Tech*. 11:4033–4058.

24 Veefkind J, *et al.* 2012. TROPOMI on the ESA Sentinel-5 Precursor: a GMES mission for global observations of the atmospheric composition for climate, air quality and ozone layer applications. *Remote Sens Environ*. 120:70–83.

25 Georgoulias AK, Boersma KF, van Vliet J, Zhang X, de Laat J. 2020. Detection of NO_2 pollution plumes from individual ships with the TROPOMI/S5P satellite sensor. *Environ Res Lett*. 15:124037.

26 Riess TCVW, *et al.* 2022. Improved monitoring of shipping NO_2 with TROPOMI: decreasing NO_x emissions in European seas during the COVID-19 pandemic. *Atmos Meas Tech*. 15:1415–1438.

27 Kaluza P, Kölzsch A, Gastner MT, Blasius B. 2010. The complex network of global cargo ship movements. *J R Soc Interface*. 7:1093–1103.

28 Boersma KF. 2008. Intercomparison of SCIAMACHY and OMI tropospheric NO_2 columns: observing the diurnal evolution of chemistry and emissions from space. *J Geophys Res: Atmos*. 113:D16S26.

29 Liu S, *et al.* 2019. An improved total and tropospheric NO_2 column retrieval for GOME-2. *Atmos Meas Tech*. 12:1029–1057.

30 Liu S, *et al.* 2020. An improved air mass factor calculation for nitrogen dioxide measurements from the Global Ozone Monitoring Experiment-2 (GOME-2). *Atmos Meas Tech*. 13:755–787.

31 Liu S, *et al.* 2021. An improved TROPOMI tropospheric NO_2 research product over Europe. *Atmos Meas Tech*. 14:7297–7327.

32 Valks P, *et al.* 2011. Operational total and tropospheric NO_2 column retrieval for GOME-2. *Atmos Meas Tech*. 4:1491–1514.

33 van Geffen J, Boersma KF, Eskes H, Maasakkers JD, Veefkind JP. 2022. TROPOMI ATBD of the total and tropospheric NO_2 data products. Royal Netherlands Meteorological Institute: Technical Report No. S5P-KNMI-L2-0005-RP issue 2.4.0.

34 Hoesly RM, *et al.* 2018. Historical (1750–2014) anthropogenic emissions of reactive gases and aerosols from the Community Emissions Data System (CEDS). *Geosci Model Dev*. 11:369–408.

35 Jalkanen J-P, *et al.* 2012. Extension of an assessment model of ship traffic exhaust emissions for particulate matter and carbon monoxide. *Atmos Chem Phys*. 12:2641–2659.

36 Ren J, Guo F, Xie S. 2022. Diagnosing ozone–NO_x–VOC sensitivity and revealing causes of ozone increases in China based on 2013–2021 satellite retrievals. *Atmos Chem Phys*. 22:15035–15047.

37 MAERSK. 2023. Advisories: operational impact of earthquake in Turkey and Syria [accessed 2023 Nov 1]. https://www.maersk.com/news/articles/2023/02/06/operational-impact-of-earthquake-in-turkey.

38 UNCTAD. 2021. Review of Maritime Transport 2021. United Nations Conference on Trade and Development (UNCTAD). Technical Report No. UNCTAD/RMT/2021 [accessed 2023 Oct 10]. https://unctad.org/publication/review-maritime-transport-2021.

39 Stein A, *et al.* 2015. NOAA's HYSPLIT atmospheric transport and dispersion modeling system. *Bull Am Meteorol Soc*. 96:2059–2077.

40 Kalnay E, *et al.* 1996. The NCEP/NCAR 40-year reanalysis project. *Bull Am Meteorol Soc*. 77:437–472.

41 Rolph G, Stein A, Stunder B. 2017. Real-time environmental applications and display system: READY. *Environ Model Software*. 95:210–228.

42 Chan KL, *et al.* 2020. MAX-DOAS measurements of tropospheric NO_2 and HCHO in Munich and the comparison to OMI and TROPOMI satellite observations. *Atmos Meas Tech*. 13:4499–4520.

43 Pinardi G, *et al.* 2020. Validation of tropospheric NO_2 column measurements of GOME-2A and OMI using MAX-DOAS and direct sun network observations. *Atmos Meas Tech*. 13:6141–6174.

44 Wang C, Wang T, Wang P, Rakitin V. 2020. Comparison and validation of TROPOMI and OMI NO_2 observations over China. *Atmosphere*. 11:636.

45 Schreier S, *et al.* 2015. Ship-based MAX-DOAS measurements of tropospheric NO_2 and SO_2 in the South China and Sulu Sea. *Atmos Environ*. 102:331–343.

46 Gelaro R, *et al.* 2017. The modern-era retrospective analysis for research and applications, version 2 (MERRA-2). *J Clim*. 30:5419–5454.

47 Crippa M, *et al.* 2023. The HTAP_v3 emission mosaic: merging regional and global monthly emissions (2000–2018) to support air quality modelling and policies. *Earth Syst Sci Data*. 15:2667–2694.

48 Janssens-Maenhout G, *et al.* 2015. HTAP_v2.2: a mosaic of regional and global emission grid maps for 2008 and 2010 to study hemispheric transport of air pollution. *Atmos Chem Phys*. 15:11411–11432.

49 Holmes C, Prather M, Vinken G. 2014. The climate impact of ship NO_x emissions: an improved estimate accounting for plume chemistry. *Atmos Chem Phys*. 14:6801–6812.

50 Vinken GC, Boersma KF, Jacob DJ, Meijer EW. 2011. Accounting for non-linear chemistry of ship plumes in the GEOS-Chem global chemistry transport model. *Atmos Chem Phys*. 11:11707–11722.

51 Guenther A, *et al.* 2012. The Model of Emissions of Gases and Aerosols from Nature version 2.1 (MEGAN2.1): an extended and updated framework for modeling biogenic emissions. *Geosci Model Dev*. 5:1471–1492.

52 Giglio L, Randerson JT, Van Der Werf GR. 2013. Analysis of daily, monthly, and annual burned area using the fourth-generation Global Fire Emissions Database (GFED4). *J Geophys Res: Biogeosci*. 118:317–328.

53 Boersma K, *et al.* 2009. Validation of urban NO_2 concentrations and their diurnal and seasonal variations observed from the SCIAMACHY and OMI sensors using in situ surface measurements in Israeli cities. *Atmos Chem Phys*. 9:3867–3879.

54 David LM, *et al.* 2019. Tropospheric ozone over the Indian subcontinent from 2000 to 2015: data set and simulation using GEOS-Chem chemical transport model. *Atmos Environ*. 219:117039.

55 Zhu L, *et al.* 2016. Observing atmospheric formaldehyde (HCHO) from space: validation and intercomparison of six retrievals from four satellites (OMI, GOME2A, GOME2B, OMPS) with SEAC^{4}RS aircraft observations over the southeast US. *Atmos Chem Phys*. 16:13477–13490.

56 Fritz TM, *et al.* 2022. Implementation and evaluation of the GEOS-Chem chemistry module version 13.1.2 within the Community Earth System Model v2.1. *Geosci Model Dev*. 15:8669–8704.

57 Xue R, *et al.* 2022. Ozone pollution of megacity Shanghai during city-wide lockdown assessed using TROPOMI observations of NO_2 and HCHO. *Remote Sens (Basel)*. 14:6344.

58 Tan Y, Wang T. 2022. What caused ozone pollution during the 2022 Shanghai lockdown? Insights from ground and satellite observations. *Atmos Chem Phys*. 22:14455–14466.

59 Lamsal L. 2011. Application of satellite observations for timely updates to global anthropogenic NO_x emission inventories. *Geophys Res Lett*. 38:L05810.

60 Vinken G, Boersma K, Van Donkelaar A, Zhang L. 2014. Constraints on ship NO_x emissions in Europe using GEOS-Chem and OMI satellite NO_2 observations. *Atmos Chem Phys*. 14:1353–1369.